PCCP

PAPER

Cite this: *Phys. Chem. Chem. Phys.*, 2015, **17**, 10135

Materials analyses and electrochemical impedance of implantable metal electrodes

Matiar M. R. Howlader,* Arif Ul Alam, Rahul P. Sharma and M. Jamal Deen

Received 16th December 2014,
Accepted 12th March 2015

DOI: 10.1039/c4cp05899b

www.rsc.org/pccp

Implantable electrodes with high flexibility, high mechanical fixation and low electrochemical impedance are desirable for neuromuscular activation because they provide safe, effective and stable stimulation. In this paper, we report on detailed materials and electrical analyses of three metal implantable electrodes – gold (Au), platinum (Pt) and titanium (Ti) – using X-ray photoelectron spectroscopy (XPS), scanning acoustic microscopy, drop shape analysis and electrochemical impedance spectroscopy. We investigated the cause of changes in electrochemical impedance of long-term immersed Au, Pt and Ti electrodes on liquid crystal polymers (LCPs) in phosphate buffered saline (PBS). We analyzed the surface wettability, surface and interface defects and the elemental depth profile of the electrode-adhesion layers on the LCP. The impedance of the electrodes decreased at lower frequencies, but increased at higher frequencies compared with that of the short-term immersion. The increase of impedances was influenced by the oxidation of the electrode/adhesion-layers that affected the double layer capacitance behavior of the electrode/PBS. The oxidation of the adhesion layer for all the electrodes was confirmed by XPS. Alkali ions (sodium) were adsorbed on the Au and Pt surfaces, but diffused into the Ti electrode and LCPs. The Pt electrode showed a higher sensitivity to surface and interface defects than that of Ti and Au electrodes. These findings may be useful when designing electrodes for long-term implantable devices.

1. Introduction

Implantable electrodes can be used to electrically stimulate impaired muscle and nerves. The electrical stimulation requires generating electrical pulses, easy routing of the pulses, and delivering effective stimulus from the electrodes to the tissue. For such applications, the electrodes with high flexibility, high mechanical fixation and low electrochemical impedance are desirable. The stringent requirements of the electrodes are the essence of high electrochemical stability and easy transfer of electrical impulses from the electrodes to ions in the surrounding electrolyte at low injected charge.[1–5] Flexibility reduces abrasive or compressive injuries and improves mechanical fixation. Low electrochemical impedance between the electrode–electrolyte (*i.e.*, tissue) is a critical requirement because it is essential in order to reduce tissue injuries, lower stimulation current (for low/no irritation) and increase the longevity of the implants.[1–3,6,7] Typically, ideal electrodes possess those characteristics and offer reversible charge transfer (Faradaic) at the electrode/electrolyte interface without provoking the host tissues, which results in safe, effective and stable stimulation. In contrast, non-ideal electrodes cause deleterious chemical changes and harmful effects due to irreversible charge transfer (non-Faradaic).[6–9]

Department of Electrical and Computer Engineering, McMaster University, Hamilton, Ontario L8S 4K1, Canada. E-mail: mrhowlader@ece.mcmaster.ca

Flexible polymer substrates such as polyimide (PI), parylene and liquid crystal polymers (LCPs) have been demonstrated for implantable electrode arrays, telemetric coils and structural membranes.[10–13] Among these substrates, LCPs have lower water absorption, a lower coefficient of thermal expansion, and higher biocompatibility.[14–17] Therefore, LCPs are regarded as some of the best implantable substrate materials, providing reliable functionality in the warm, moist, and mobile environment of the human body.

A wide range of materials, including titanium (Ti), platinum (Pt) and gold (Au), have been used for implantable electrodes[7] because of their high biocompatibility, high charge transfer capability and low/non-reactivity in the *in vivo* environments.[18–22] Electrodes made of these materials have been tested in phosphate buffered saline (PBS) solution to mimic the operating environment of the implants. While Ti is used as an electrode and adhesion material on polymers,[23] the oxidation of Ti[24] in the implantable environments may degrade its performance. Also, the oxidation of Pt,[25] the oxygen reduction of Au[26] and Pt, and their electrolysis in water[25,26] degrade the reversible charge transfer capability of the long-term implanted electrodes and damage surrounding tissues. Therefore, the electrochemical impedance of Pt–Ti electrodes on flexible substrates was increased in PBS solution.[27,28] Also, the Au electrode covered with poly(3,4-ethylenedioxythiophene) doped poly(styrene-sulfonate) (PEDOT:PSS) on a copper laminated Kapton® PI substrate

showed higher stability in its electrochemical impedance properties than that of a bare Au electrode dipped in saline for 40 days.[29] Furthermore, an increase in the impedance at the electrode interface was reported due to the foreign body reaction with organisms.[30] Therefore, the operating environment, and the type of polymer substrates, electrode materials and surface/interfacial adhesion layers affect the performance of the implantable electrodes.

Recently, we observed the change of electrical impedance for Pt, Au and Ti electrodes on LCPs after long-term-immersion in PBS.[1,3] The impedance behavior was investigated through analyzing the surface roughness and the double layer capacitive (signified as β) behavior of the electrodes. The roughness of the Au electrode was significantly increased as compared to Ti. The value of β significantly dropped for the Pt and Ti electrodes as opposed to the Au electrodes. The significant decrease of the β value was induced by the prolonged immersion in PBS. The increase of the impedance of the electrodes was believed to be due to the amount of hydroxyls on the surface.[1,31] Also, the increased surface roughness was also attributed to the increase in the interfacial electrochemical impedance of the electrode. Moreover, the physical changes in the chemical environment on the surface and inside the immersed Au, Ti and Pt electrodes (*i.e.*, pores due to chemical elements of PBS)[32–35] may control the interfacial impedance of the electrode–electrolyte. To the best of our knowledge, there is no experimental observation on the surface wettability, surface and interface defects and the elemental depth profile to explain the change of the impedance of the implantable electrodes after long-term PBS immersion. These queries are critical to address design challenges for the longevity of implantable devices.

This article investigates the cause of changing electrochemical impedance of long-term PBS-immersed Au, Ti and Pt electrodes on LCPs. We measured the water contact angle using a drop shape analyzer, analyzed defects using a scanning acoustic microscope, and observed chemical elements using an X-ray photoelectron spectroscope to investigate the impedance change mechanisms of these electrodes. These results were correlated to understand the increased impedance that would provide important insights about long-term implanted electrodes.

2. Experiments

2.1. Fabrication of flexible electrodes

For this study, we used the Pt, Ti and Au electrodes fabricated on LCP substrates that were used for electrochemical impedance measurements after dipping for 42 days in PBS solution in our previous study.[1,3] In fact, we measured the electrochemical impedances for the electrodes dipped for 1, 3, 7, 14, 21, 28, 35 and 42 days. After 42 days of immersion, we observed significant changes in the impedance as opposed to other shorter (*e.g.*, 21 days) immersion time.[1] Ti was used as the adhesion layer between the substrate and the electrode. The thicknesses of the adhesion layer and the electrode were 30 and 200 nm, respectively (Fig. 1(a)). The electrode was deposited by a low cost process[36] on the LCP substrate of a size of about (15 mm × 15 mm) that was cut from an A4 size LCP sheet. A 100 μm thick copper mask with a hole of 8 mm diameter was placed on top of the LCP during the deposition. So the diameter of the electrode would be around 8 mm. The adhesion and

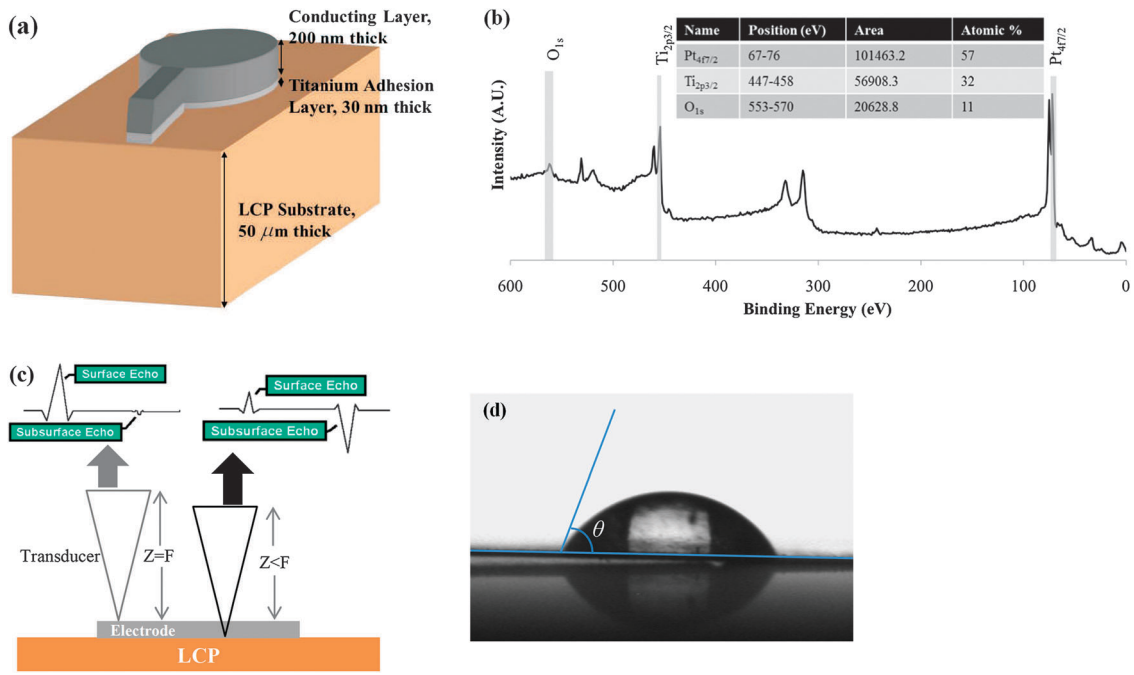

Fig. 1 (a) Schematic diagram of the deposited electrode on the LCP substrate. (b) Peak area quantification method for atomic percentage calculation from XPS wide scan spectra using CasaXPS.[41] (c) Focusing diagram in Scanning Acoustic Microscopy (SAM).[40] (d) Contact angle measurement using the sessile drop technique.

conducting layers were deposited using electron beam evaporation. The deposition rate was 1.5 Å s^{-1} and the background pressure was 1×10^{-4} Pa. The purities of the Pt, Au and Ti targets were 99.99%, 99.999% and 99.99% respectively. All the deposition conditions such as the target location, sample location, target parameters, and chamber conditions were kept constant for the deposition of all electrodes and no post-deposition heat treatments were used. The electrodes dipped in PBS were not encapsulated. The three-electrode electrochemical impedance spectroscopy (EIS) was performed using a Gamry framework workstation.[1,3] An alternating current excitation with a voltage of 10 mV was used at a frequency range from 0.1 Hz to 100 kHz. Equivalent circuits and parameters were determined with ZPlot software. Further details of the LCP substrate, fabrication of electrodes and impedance measurements can be found in ref. 1, 4 and 37.

2.2. Contact angle measurement

The water contact angle was measured using a drop shape analysis system (DSA100) from KRÜSS with a 5 μl de-ionized water droplet using the sessile drop method (Fig. 1(d)).[38,39] The water contact angle shows the affinity of the surface for hydroxyl groups. The contact angles of each specimen were measured once every 2 seconds for 2 minutes of elapsed time to achieve an average contact angle.

2.3. Scanning acoustic microscopy

Acoustic microscopy is a non-destructive testing method of defects through high-resolution imaging of objects created by high frequency ultrasound. The sound waves are captured either when passing through (transmission mode) or echoing back (reflection mode) from an object.[40] A digital image is generated by digitizing those sound waves. Therefore, any internal structures and defects present in the objects are identified. The Scanning Acoustic Microscopy (SAM) in this article was done using GEN5™ C-SAM® from Sonoscan® with a high frequency (230 MHz) Surface Wave transducer (230 SW). We observed surface and interface defects of the electrodes with a resolution of 4 microns (Fig. 4). During scanning, the first echo encountered is called the surface echo (Fig. 1(c)). At this position, the distance between the bottom of the transducer and the top of the specimen (Z) is approximately equal to the focal length of the transducer (F). It provides the surface profile of the specimen. As the transducer is moved closer to the surface and the focus moves into the specimen (*i.e.*, $Z < F$), a second echo will start appearing to the right of the surface echo and increase in amplitude (Fig. 1(c)). Focusing up and down helps to observe any changes at the boundary between two materials, *e.g.*, defects between the electrode adhesion layer and the polymer.

2.4. X-ray photoelectron spectroscopy

X-ray photoelectron spectroscopy (XPS) spectra were acquired using the JPS-9200 from JEOL. The Magnesium (Mg-α) X-ray source with 10 keV and 15 mA was used for acquiring wide-scan and narrow-scan spectra with a binding energy resolution of 0.1 eV. Also, the Ar-ion etching (with 3 keV and 20 mA) was done with 0.08 Pa pressure. The XPS instrument was calibrated using an Au sample.[31]

Depth profile XPS spectra of Ti, Pt and Au electrodes were quantified in terms of the peak intensities, areas and positions of different elements. Generally, the peak intensities signify the amount of a particular element, whereas the peak positions suggest the elemental and chemical composition. In this experiment, we measured the atomic concentration of each element by calculating the area of the quantification region (shaded area in Fig. 1(b)) using CasaXPS software.[41] Fig. 1(b) illustrates a survey spectrum of the Pt electrode where the atomic concentration was calculated based on the area of the quantification regions as shown in the quantification table (inset). Auger peaks (*e.g.*, Na_{KLL}) were not considered in the calculation of the atomic concentration of the chemical elements. The quantification regions were specified by selecting an appropriate range of energies as well as subtracting background signals.

All specimens showed a charging effect due to the dielectric nature of the LCP. Charge corrections were accomplished using $Au_{4f_{7/2}}$, $Pt_{4f_{7/2}}$ and O_{1s} for Au, Pt and Ti electrodes, respectively. $Au_{4f_{7/2}}$ and $Pt_{4f_{7/2}}$ were chosen as references for the charge correction due to their non-oxidizing behavior. On the other hand, O_{1s} was taken as the reference for Ti because of its oxidizing nature.

3. Results and discussion

3.1. Electrical impedance of the electrodes

Following our previous study on the electrochemical impedance of Au, Ti and Pt electrodes immersed in PBS solution up to 42 days at room temperature,[1,3] we extracted their impedances as a function of frequency only for ''Day 1'' and ''Day 42'' to investigate the fundamental mechanism responsible for the change in the impedance of long-term immersed implantable electrodes. Fig. 2 shows the electrochemical impedance of Au, Ti and Pt electrodes immersed in PBS solution for ''Day 1'' and ''Day 42''. After 42 days of immersion, the impedances of the electrodes were increased at higher frequencies (*i.e.*, above 1 Hz) which is in contrast to the impedance of the Au electrode on nickel phosphorus/copper/PI.[29] For Au, the cut-off frequency was shifted to higher frequency. In the case of Ti and Pt, no significant cut-off frequency was observed. The change of impedances for ''Day 42'' compared to ''Day 1'' may be correlated with the chemical compositions and surface/interface behavior of the electrodes and their capacitive interfacial behavior (β).[1,3] For a pure capacitor, the value of β is 1. In our previous study,[1] we observed that the value of β for ''Day 42'' Au was 0.85, but for Ti and Pt, it was 0.25 and 0.38, respectively. Also, the values of the constant phase element capacitance, K (at angular frequency, $\omega = 1$ rad s^{-1}), for Ti and Pt were decreased significantly at ''Day 42'' as compared to Au. These significant drops in β and K values for Pt and Ti electrodes as compared to that of Au imply that distinct mechanisms were associated with the oxidation and reactivity

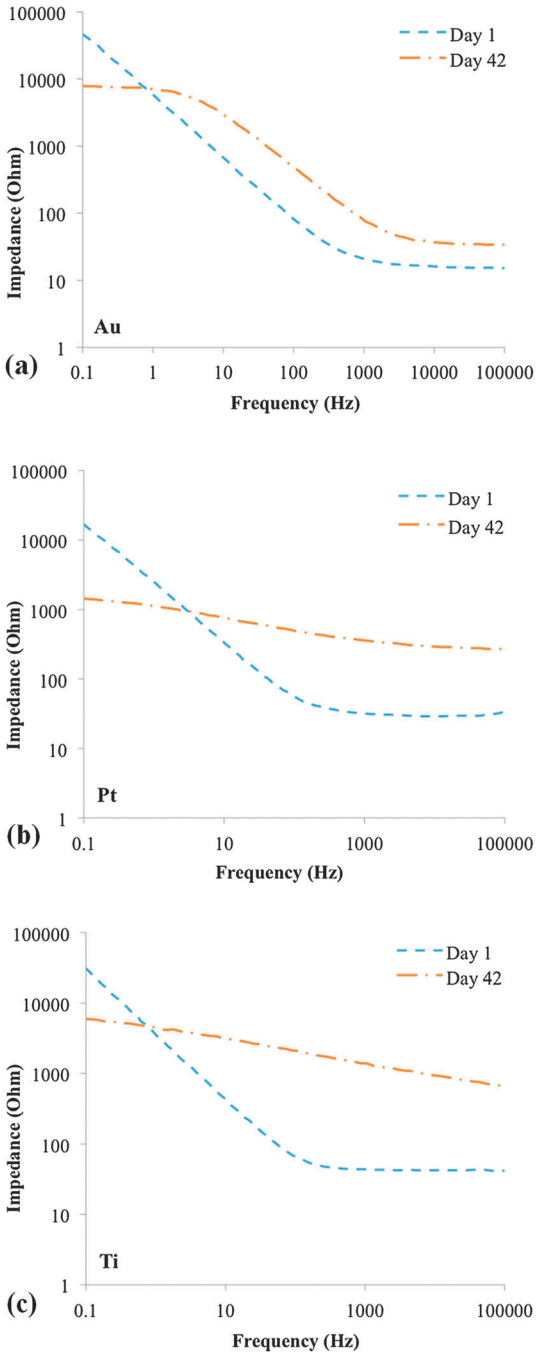

Fig. 2 Electrochemical impedance of (a) Au, (b) Pt and (c) Ti electrodes immersed in PBS solution for "Day 1" and "Day 42" as a function of frequency.[1] The diameters of the electrodes are 8 mm.

of the surface and interfaces of the electrodes.[1,42] Therefore, we focused only on the "Day 42" electrodes to identify the surface wettability, surface and interface defects, and elemental compositions towards understanding the increase of impedance.

3.2. Surface wettability of the electrodes

The water contact angle quantifies the wettability of a solid-state surface. Hence, this is critical to understand the reactions of the PBS solution with the electrode surfaces. A higher contact angle renders a hydrophobic surface. In contrast, a lower contact angle indicates a hydrophilic surface.[43] In general the demarcation line between these two surfaces is the contact angle in the ranges of 30°–45°.[31,44] Our results show that the contact angle for Ti electrodes is 54°. After 2 min, the contact angle decreases to 45° (Fig. 3). On the other hand, the contact angle for Pt starts at 94° and after 2 minutes it decreases to 76°. Also, the contact angle of Au starts at 72° and becomes 66° after two minutes. Therefore, the contact angles of Pt and Au electrodes indicate that they are more hydrophobic than the Ti electrode.

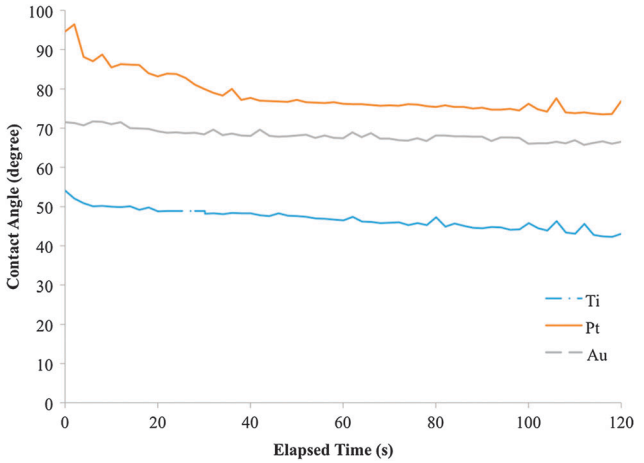

Fig. 3 Contact angle variation with time for the Au, Pt and Ti electrodes after immersing for 42 days.

Surface roughness and porosity control the water contact angle.[31,45,49] In our previous study, we found that the surface roughness of Au, Pt and Ti electrodes on LCPs before immersion in the PBS solution was 3.18, 3.44, and 4.49 nm, respectively.[1] After immersion in the PBS solution for 42 days, the roughness of Au and Ti was 11 and 6.03 nm, respectively. The surface roughness of Pt was not measureable due to delamination from LCPs. The higher contact angle for Au than that of Ti may be due to its high surface roughness and adsorbed hydrophobic contaminants.[46] One of the examples of the contaminants would be Na that comes from the PBS solution. Also, the high contact angle of Pt may be attributed to its high surface roughness. On the other hand, the low surface roughness of Ti and its high reactivity to alkaline and oxides resulted in a reduced contact angle with a high number of pores.[47] The high surface roughness of the Pt electrode and the high number of pores of the Ti electrode are responsible for their non-ideal (*i.e.*, $\beta \ll 1$) capacitive behavior.[48]

3.3. Surface and interface defects of the electrodes

Fig. 4(a) shows the SAM image for the top surface of an Au electrode that has been immersed for 42 days in PBS solution. The image shows four things: (1) the white area is the electrode area showing the surface topography, (2) the square black mark is the ion etching area resulting from the depth profile experiments (as given in the Section 3.3), (3) the big black dots due to the delamination of Au and (4) the small dots over the white

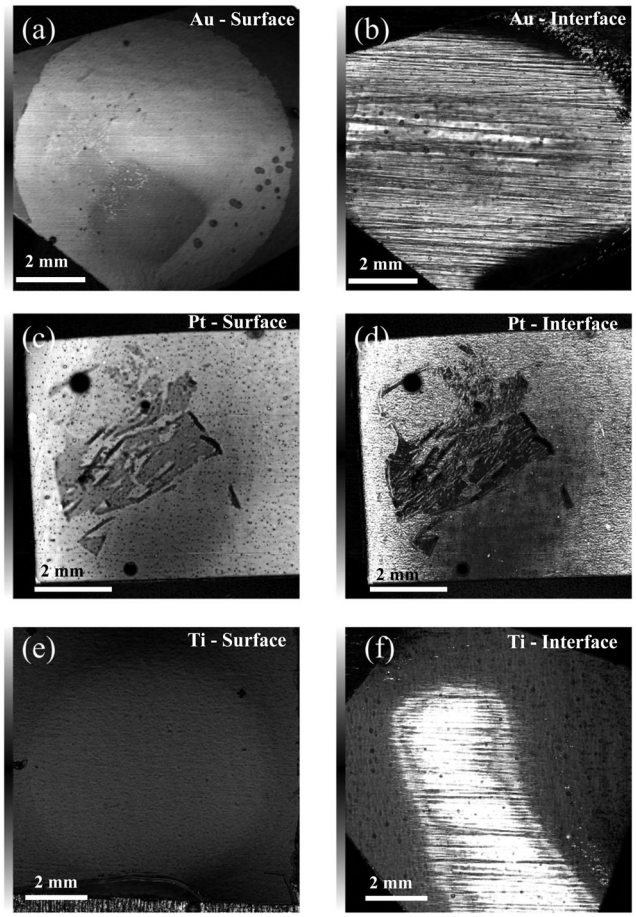

Fig. 4 Scanning acoustic microscope (SAM) images of (a) the top surface of Au on LCPs, (b) the interface of Au/LCP, (c) the top surface of Pt on LCPs, (d) the interface of Pt/LCP, (e) the top surface of Ti on LCPs, and (f) the interface of Ti/LCP.

area are a result of defects due to the prolonged immersion in PBS solution.

Fig. 4(b) shows the SAM image of the interface of the long-term immersed Au electrode. Small holes are observed over the ion treated area. Ion etching induces these defects. Also, these defects do not match with that of the surface. Therefore, these are likely to be artifacts rather than interfacial pores. The big dots seen in Fig. 4(a) are being shadowed in Fig. 4(b). In Fig. 4(b), the identified white area is due to the bending of the specimen. The density of defects in the ion etched and non-etched areas is identical. The defects in the ion-etched area are more visible than those of the non-etched area. This may be attributed to the thinner layer of Au caused by ion etching.

Fig. 4(c) and (d) show the top surface of the Pt electrode and the interface of Pt/LCP, respectively. The specimen surface shows Pt delamination. This delamination is due to the reactivity of the adhesion layer with the PBS solution (*i.e.*, sodium chloride, sodium phosphate, potassium phosphate and potassium chloride). In comparison to the Au electrode, the Pt electrode shows a smaller but higher density of pores. The majority of the pores are identical in size. The surface pores are connected to that of the interface of Pt/LCP, as shown in Fig. 4(d). However, a couple of large sized defects are observed which could be some artifacts.

Fig. 4(e) and (f) show the top surface of the Ti electrode and the interface of Ti/LCP, respectively. The top surface of Ti shows few pores. The white area of the Ti/LCP interface (Fig. 4(f)) is due to bending of the specimen. The interfacial pores are observed all over the interfacial area.[49] The sizes of the pores are identical to that of the Au/LCP interface, but larger than that of the Pt/LCP interface.

The surface pores and oxides can be correlated with the hydrophilicity and hydrophobicity of the surfaces. The lower contact angle of the Ti electrode could be due to the higher alkaline and oxides on the surface. In contrast, the higher contact angle of the Pt electrode than that of Au and Ti may result from the higher number of pores on the surface. Au also has a higher number of pores on the surfaces than that of Ti, which can be correlated with the higher contact angle and higher surface roughness.[48] On the other hand, the Ti/LCP interface has a greater number of pores than that of Pt and Au. This behavior indicates that the bulk of the Ti electrode is also prone to the alkaline and oxides as compared to Au and Pt resulting in higher pores in the Ti electrode. These pores may be permeable to defects favoring the diffusion of the electrode materials into the LCP[49] and resulting in varying defects across the depth of the electrodes. Therefore, the elemental distribution of the electrodes could be associated with their oxidation and diffusion behavior.

3.4. Elemental analysis of the electrodes

3.4.1 Depth profile of the Au electrode. Elemental analysis of the surface and interface has been investigated to understand the role of the chemical compositions in the changes in the electrochemical impedance of the electrode. Fig. 5 shows the (a) wide scan spectra as a function of etching time and (b) the depth profile of the Au electrode dipped in PBS dipped for 42 days. The etching step was 60 s. The major peaks identified were Au_{4f}, Ti_{2p}, O_{1s} and C_{1s}. Before etching (0 s), two strong peaks of Au_{4f}, two moderately strong peaks of Au_{4d} and a weak peak of Au_{4p} were observed. No carbon was detected on the surface. Also, an Auger peak for Na_{KLL} was observed. The peak positions for the peak near O_{1s}, and Na_{KLL} were 514 and 262 eV, respectively.[50,51] Since Au does not oxidize, the peak near O_{1s} could be due to the oxidation of Na_{KLL} adsorbed on the surface. After 60 s of etching, oxygen and Alkali disappeared. All the peaks for Au became stronger. After 1080 s of etching, Ti appeared and Au became weaker. After 3000 s of etching, all other peaks disappeared except Au_{4f}, but remained as a weak peak. A strong peak for carbon appeared from LCP.

The detailed elemental distribution in atomic concentration as a function of etching time can be seen in Fig. 5(b). Before etching, Au was highest followed by oxygen. Au increased after etching for 60 s and remained constant until 780 s. Then Au decreased and Ti increased with the increase of etching time. Ti peaked at 1140 s. From 960 s, oxygen started appearing, then increased and peaked at 1260 s. Carbon began to appear from 1140 s, then gradually increased, and finally saturated around 2000 s. The depth profile

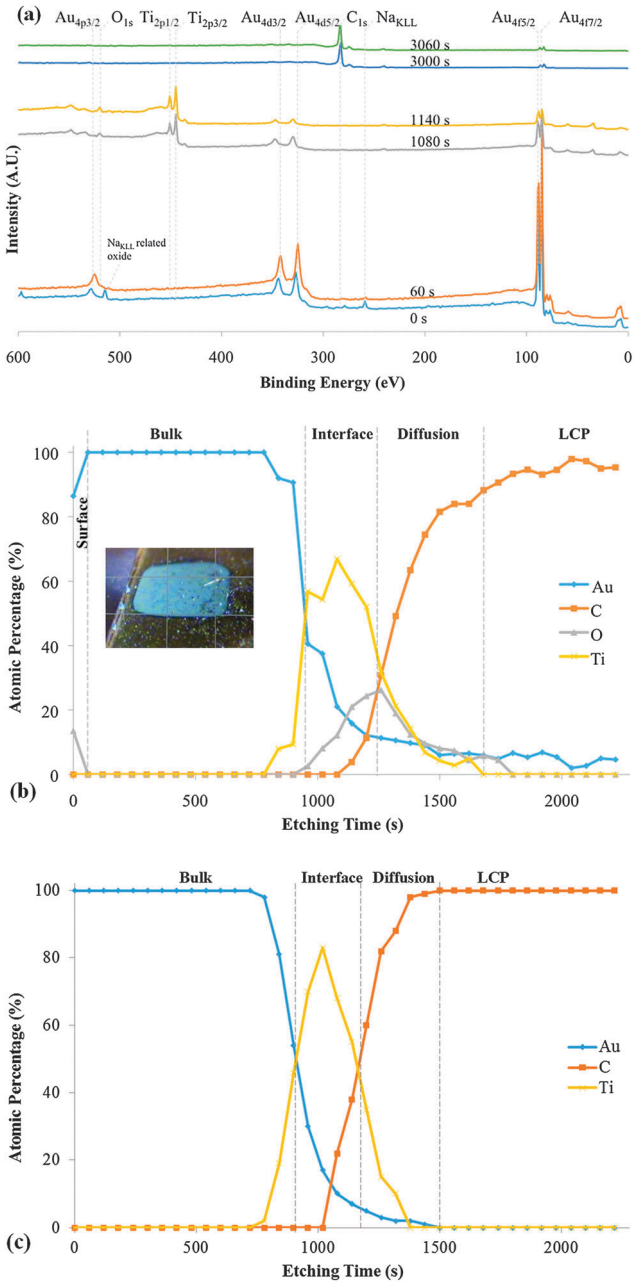

Fig. 5 (a) XPS wide scan spectra during etching for the Au electrode. (b) Depth profile of the Au electrode, with the optical image of the etched Au electrode. The white area of the optical image on the inset shows the top surface of the Ar-ion etched Au electrode. (c) Depth profile of the pristine Au electrode (*i.e.*, without PBS immersion).

indicates an interfacial region between 840 s and 1800 s that consists of curves for oxygen and Ti with almost Gaussian shapes, and decreasing and increasing curves for Au and C, respectively. The curves for Ti and oxygen indicate that the adhesion layer underneath the Au electrode was completely oxidized. Also, Au was detected even after the complete elimination of the Ti and O signals. The disappearance of the O signal in the Au electrode may indicate the replacement of oxygen from LCPs due to the diffusion of Au into LCPs. Based on the estimated etching rate of the Au electrode (*i.e.*, ~0.22 nm s^{-1}), the interface and the diffusion depth would be 65 and 100 nm, respectively. This depth is larger than the thickness of the adhesion layer (*i.e.*, 30 nm). This discrepancy could be due to the different etching rate of Au at the interfacial region where Au, Ti, C and O are diffused together. However, the cause of the diffusion of Au into LCP is not known from this study.

In order to understand the route for the oxidation, we investigated the depth profile of the Au electrode before immersing into PBS, as shown in Fig. 5(c). The pristine Au electrode clearly shows Au, Ti and C at the interfacial region without any oxidation. This indicates that the interfacial oxides observed in the electrodes immersed for 42 days (Fig. 5(b)) did not originate from the fabrication process of the electrodes.

The literature has shown that adhesion layers with the types of deposited materials and chemical elements for the electrodes control the surface and interface properties of the electrodes–electrolytes.[52–54] The effect of the Cr adhesion layer between gold electrodes and quartz was investigated from the response of an electrochemical quartz crystal microbalance (EQCM) in $HClO_4$ and phosphate buffer.[52] The gold electrode in the buffer solution was attacked by oxygen chemisorption and further it was dissolved in the presence of a small amount of chloride. Gold films were contaminated due to the poor Cr adhesion layer. Also, a significant amount of extraneous metal atoms was present on the gold electrode surface. However, the gold electrode with a Ti adhesion layer showed negligible dissolution of gold. In an electrochemical study of gold electrodes with anodic oxide films, it was found that two monolayers of anodically formed gold oxides on the surface completely inhibited electrochemical redox reactions.[53] Furthermore, the gold electrode was electrically characterized with a thiol self-assembled monolayer (SAM) for biosensing applications.[54] A cyclic voltammogram of the fresh gold electrode before and after thiol deposition in PBS showed that the oxidation reaction at the interface was reduced after thiol deposition and no further reduction was taken place.[54] Therefore, these results support the presence of alkali materials on Au electrodes and the absence of alkali inside the electrode surface due to strong adhesion of Au and Ti with LCPs.

3.4.2 Depth profile of the Pt electrode. Fig. 6(a) shows the wide scan spectra during the depth profile of the Pt electrode immersed in PBS for 42 days. The spectra contain Pt_{4f}, Pt_{4d}, Ti_{2p}, O_{1s} and C_{1s} peaks. Before etching (0 s), peaks for Pt_{4f}, Na_{KLL} (Auger) and O_{1s} with identical intensities were observed. Also, the Pt_{4d} peak with lower intensity compared to other peaks was observed. No carbon was detected on the surface. This behavior is similar to that of the Au surface. Ar ion etching of the Pt surface for 60 s eliminated the oxide and alkaline elements. In this step, a new peak for Pt_{4p} and the high intensity peaks for Pt_{4f} and Pt_{4d} were observed. After 960 s of etching, Ti and oxygen appeared, and Pt signals became weaker than that of the 60 s etched surface. After 1860 s of etching, all other peaks disappeared except C_{1s}. This high intensity peak may be due to the carbon from LCPs.

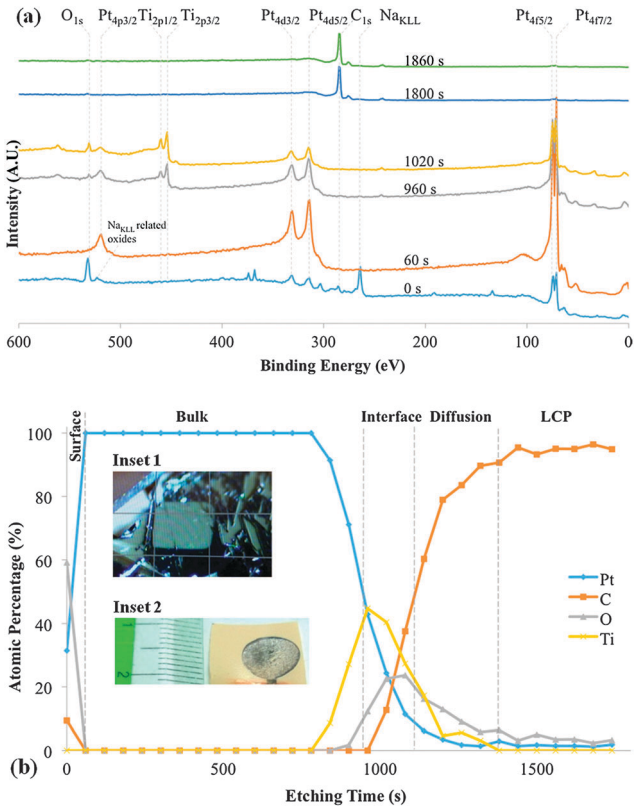

Fig. 6 (a) XPS wide scan spectra during etching for the Pt electrode. (b) Depth profile of the Pt electrode with the optical image of the etched Pt electrode. The white area of the optical image on the inset 1 shows the top surface of the Ar-ion etched Pt electrode. Inset 2 shows the delamination of the Pt electrode after immersion in PBS.

In the depth profile (Fig. 6(b)), the atomic concentration of carbon before etching of the Pt electrode was highest followed by oxygen and carbon. After etching the Pt electrode surface for 60 s, oxygen disappeared completely and Pt remained constant until 780 s. Then Pt started to decrease with the increase of etching time. At that stage, Ti started to appear and peaked at 960 s. After 840 s of etching, oxygen again appeared and peaked at 1080 s. Carbon appeared from 1020 s, then gradually increased, and finally saturated around 1700 s. The increase of Ti was followed by the increase of oxygen and carbon, but Pt was decreased with the increase of etching time. All the curves were intersected at an interfacial region between 780 and 1380 s. In this region, Ti and oxygen showed curves with shapes of Gaussian distribution. Also, decreasing and increasing curves for Pt and C, respectively, were observed. After that, Ti was terminated but Pt, C and O were detected. The elimination of Ti in the Pt electrode is similar to that in the Au electrode. Also, while the Pt detection in LCPs is similar to that of Au, the O signal was present in the LCP of the Pt electrode. This behavior may indicate the diffusion of Pt into LCPs. The interface and diffusion depth for Pt would be 40 and 60 nm, respectively, if we follow the similar calculation (*i.e.*, etching rate = 0.22 nm s^{-1}) as Au. Again the observed depth is larger than the thickness of the adhesion layer (*i.e.*, 30 nm) that may be attributed to the identical phenomena to that of the Au electrode.

A few monolayers of the Pt surface (Fig. 6(a)) were oxidized rather than the complete oxidation of the inner layers (bulk). These results are identical to the cyclic voltammogram study of Pt electrodes in PBS solution with dissolved oxygen at a potential range of −1.0 V to +1.7 V.[55] Formation and reduction of oxide and adsorption and desorption of hydrogen were observed. In addition, the oxidation of chloride ions, and the oxidation and reduction of phosphate groups were found.[55] In another study, the electrochemistry of Pt electrodes in PBS showed the role of bovine serum albumin (BSA) in oxygen reduction and electrode dissolution of the Pt electrode.[56] It was found that irreversible O_2 and H_2 evolution occurs in the presence of BSA when applying shorter pulses resulting in inhibited Pt dissolution. On the other hand, the inhibitory effect of O_2 reduction may change with deoxygenated BSA-containing PBS. Identical results on the formation and reduction of oxide and adsorption and desorption of hydrogen were reported in the cyclic voltammogram study of the Pt electrode in PBS in ref. 1. However, the XPS results from this study on the surface oxidation of Pt do not support the hydrophobicity (contact angle is 94°) identified in the water contact angle measurements. The high contact angle may be due to the scattered surface oxide of Pt instead of being continuous. Therefore, the top layers of the Pt electrode act as the hydrophobic surface.

In fact, the depth profile indicates isolated oxide layers of the adhesion layer at the interface between the bulk (Fig. 6(b)) and LCPs. Also, only the Pt electrode of the three electrodes was delaminated. Furthermore, the optical image of the Pt electrode shows higher delamination on the areas other than that of the edges (Fig. 6(b), Inset 2). This delamination may be associated with the significant number of pores (Fig. 4(c)) created through the scattered surface oxide (Fig. 6(a)). The chemical elements (Alkali) of the PBS solution permeate through the pores and attack the oxidized adhesion layer of the Pt electrode system. On the other hand, the adhesion layer in the Au electrode system without immersing in PBS (Fig. 5(c)) was not oxidized. Therefore, this study does not provide evidence whether the contact between the electrolyte and the Ti adhesion layer causes the corrosion of the Ti adhesion layer. In fact, the purity, processing conditions and surface porosity of the electrodes may control the corrosion behavior.

3.4.3 Depth profile of the Ti electrode. Fig. 7(a) shows the wide scan spectra during the depth profile of the Ti electrode immersed in PBS for 42 days. The spectra contain Ti_{2p}, O_{1s} and C_{1s} peaks. Before etching (0 s), peaks for Ti_{2p}, Na_{KLL} (Auger) and O_{1s} were observed. Also, Ti_{3p} and Ti_{3s} peaks with relatively lower intensity compared to other peaks were observed. No carbon was detected on the surface. In contrast, Ti had the penetrated Alkali throughout the adhesion and electrode to the LCP. Ar ion etching of the Ti surface for 60 s could not eliminate the oxide and alkaline elements. After 1500 s of etching, the oxygen peak became stronger, and Ti peaks became weaker than that of the 60 s etched surface. After 2400 s of etching, all other

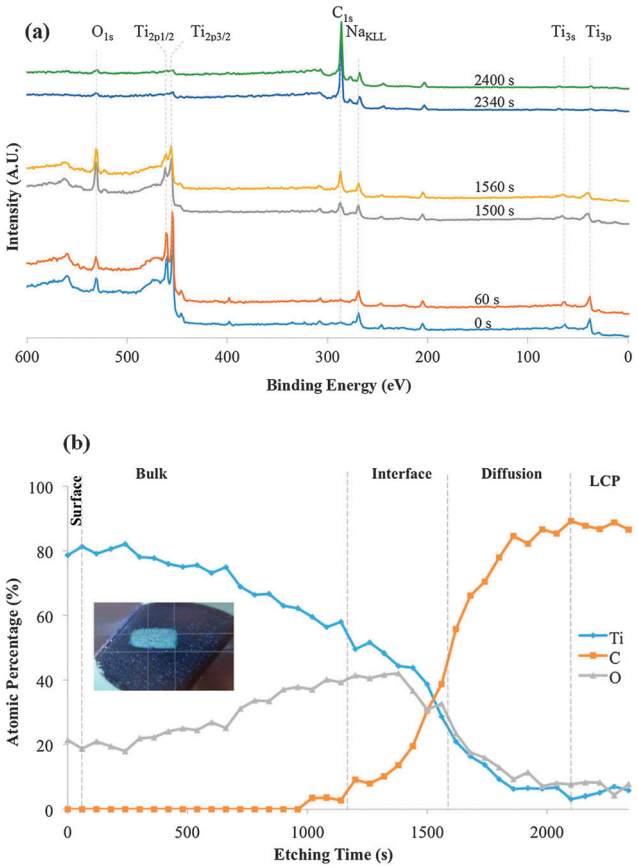

Fig. 7 (a) XPS wide scan spectra during etching for the Ti electrode. (b) Depth profile of the Ti electrode with the optical image of the etched Ti electrode. The white area of the optical image on the inset shows the top surface of the Ar-ion etched Ti electrode.

peaks disappeared except C_{1s}. This peak with high intensity may be due to carbon appearing from the LCP.

In the depth profile (Fig. 7(b)), the atomic concentration of Ti was higher than that of oxygen before etching and after 1500 s of etching. However, there was a gradual increase of oxygen and *vice versa* for Ti until 1500 s of etching. After 1560 s of etching, the amount of oxygen became higher than that of Ti and both the peaks became diminished. Carbon started appearing from 960 s, then gradually increased, and finally saturated around 2100 s. All the curves were intersected between 1500 s and 1560 s. Since both the electrode layer and adhesion layer were made of Ti, the interfacial region appears to be broader between 960 s and 2100 s. In this region, decreasing and increasing of Ti and C, respectively, were observed. Na_{KLL} was detected even after the elimination of Ti (Fig. 7(a)). This behavior may indicate the diffusion of alkaline elements into LCPs. A similar calculation for the interface and the diffusion depth of Ti (etching rate = 0.20 nm s^{-1}) to that of the Au and Pt electrodes shows that it would be about 85 and 100 nm, respectively. The depth of the interface is larger than the thickness of the adhesion layer (*i.e.*, 30 nm), which may be due to the different etching rate of diffused Ti, C and O at the interfacial region.

The XPS results reveal continuous oxidation of the Ti electrode and the adhesion layer. This behavior may be comparable to that in the extracellular electrolyte that is separated from the electrode by a molecular layer of water adsorbed on the metal surface.[35] In the literature, it is shown that the passive oxide film can be formed on Ti electrodes immersed in PBS with a significant increase of electrical resistance.[24,57,58] The increase of the electrical resistance was reported due to the passivation of oxides, growth of oxides and partial reduction of Ti.[48,58] The depth profile results also show that Ti diffuses in LCPs. This diffusion may be due to the presence of pores in the inner layers of the Ti electrode.[24]

Table 1 summarizes the chemical compositions of Au, Pt and Ti in atomic concentration at different positions across the depth of the electrodes. The binding energy for the O_{1s} peak on the Au surface was observed to be 514 eV, which is different from that of Ti (531 eV) and Pt (533 eV). The oxide peak on Au is due to the oxidation of Na_{KLL} adsorbed on the surface.[50,51]

Table 1 Summary of the chemical compositions of Au, Pt and Ti in atomic percentage at different positions across the depth of the electrodes

Electrodes	Elements	Binding energy (eV)	Atomic percentage (%) of elements at positions with respect to electrodes				Diffusion of adhesion layer (Ti) into LCP	Electrode diffusion into LCP	Interface (nm)	Diffusion (nm)	Remarks
			Surface	Bulk	Interface	LCP					
Au	O_{1s}	514	14	0	0–26	0	None	Yes	65	100	Discontinuous adhesion layer
	C_{1s}	284	0	0	0 → 90	93–97					
	$Ti_{2p_{3/2}}$	445	0	0	8–59	0					
	$Au_{4f_{7/2}}$	85	86	100	92 → 6	3–7					
	Na_{KLL}	262	Yes	None	None	None					
Pt	O_{1s}	533	59	0	2–24	6 → 3	Yes	Yes	40	60	Discontinuous adhesion layer
	C_{1s}	285	9	0	0 → 90	90 → 95					
	$Ti_{2p_{3/2}}$	455	0	0	3–44	3 → 2					
	$Pt_{4f_{7/2}}$	71	32	100	91 → 2	1–2					
	Na_{KLL}	265	Yes	None	None	None					
Ti	O_{1s}	531	21	18 → 38	37 → 7	~7	Yes	Yes	85	100	Continuous adhesion layer
	C_{1s}	285	0	0	4 → 89	~88					
	$Ti_{2p_{3/2}}$	456	79	81 → 62	59 → 4	~5					
	Na_{KLL}	270	Yes	Yes	Yes	None					

On the other hand, the O_{1s} peak for Ti and Pt was due to the oxidation of the electrode surfaces. A comparison in the change of the chemical compositions for the Ti electrode at the surface, bulk, interface and LCP shows that the electrode material gradually oxidizes and diffuses into LCPs. In contrast, the adhesion layer oxidizes in the Au and Pt electrodes that localize and stop diffusion of oxygen and carbon from LCPs. For all the electrodes, electrode materials were diffused into LCPs. The approximate widths of the interfacial regions for Au, Pt and Ti electrodes were 65, 40 and 85 nm, respectively. The largest interfacial width for Ti is due to the ease of diffusion in the Ti electrode system through the highest number of pores and its continuous oxidation. On the other hand, the non-oxidation of Au and Pt electrodes and the localized oxidation of the adhesion layer in their electrode systems were responsible for the narrower diffusion depth.

4. Impedance change mechanisms

Previously, the impedance change for the long-term-PBS-immersed (Day 42) Au, Pt and Ti electrodes has been explained using the estimated parameters for the empirical constant (*i.e.*, β) and the double layer capacitance (*i.e.*, $C_{dl} = K$) of the constant phase element as described in eqn (1) and (2).[1,3,42]

$$Z_{CPE} = \frac{1}{j\omega C_{dl}} \approx \frac{1}{K(j\omega)^{\beta}} \quad (1)$$

$$f_c = \frac{1}{2\pi R_e K} \quad (2)$$

where, Z_{CPE}, ω, f_c, and R_e are the constant phase element (CPE) impedance, angular frequency, cut-off frequency and electrolyte resistance, respectively (Fig. 8). The β and K parameters deviated from the ideal values due to the hydrolytic attack on the electrodes. However, the underlying physical and chemical mechanisms for the impedance change were not known. The surface wettability, surface-interface defects and elemental depth profile results discussed in this article provide us with useful insights into the mechanisms. While the impedances in the lower frequencies (below 1.2 Hz for Au, 1.3 Hz for Ti and 12 Hz for Ti) changed into lower values, the impedances at higher frequencies changed into higher values compared with that of "Day 1".

The changes in the impedance in the lower and higher frequency ranges are attributed to the behavior of the surface, bulk and interface of the electrodes. The total impedance of the equivalent circuit for the model shown in Fig. 8 can be expressed by,[4]

$$Z_{total} = R_e + R_{ct}||\frac{1}{j\omega C_{dl}} = (R_e + R_{ct})\left(\frac{1 + j\omega\left(\frac{R_e R_{ct} C_{dl}}{R_e + R_{ct}}\right)}{1 + j\omega(R_{ct} C_{dl})}\right) \quad (3)$$

At lower frequencies, the double layer capacitance (C_{dl}) behaves as an open circuit (from eqn (3)). Therefore, for "Day 1", the equivalent impedance (Z_{total}) of the electrodes at lower frequencies becomes approximately $R_e + R_{ct}$. For "Day 42", the oxidation behavior in the electrode systems may affect C_{dl} that can reduce Z_{CPE}. This behavior is supported by the distinct parameters of β and K for Au, Pt and Ti electrodes. While β and K values for the Au electrode after 42 days immersion in PBS were not significantly changed, these values for the Pt and Ti electrodes were considerably reduced.[1] Also, R_{ct} is dominant at lower frequencies and it is lower than Z_{CPE} for "Day 42". Then the resulting parallel impedance of R_{ct} and Z_{CPE} for "Day 42" is reduced than that of "Day 1" at lower frequencies. It is worth noting that the value of R_e for all the electrodes varies between 18 and 55.2 Ω[3] and may remain unchanged with immersion time. Therefore, the impedance of the electrodes at lower frequencies for "Day 42" is lower than that of "Day 1". At high frequencies, on the other hand, C_{dl} dominates the impedance. Then the equivalent impedance of the electrodes at high frequencies is approximately the electrolyte resistance (R_e) in series with Z_{CPE}.

Although the water contact angle is dependent on the surface behavior such as surface roughness and adsorbed contaminants, it does not have a straightforward relationship with the impedance of the electrodes. The high water contact angle of Au may be attributed to its non-oxidation and high surface roughness.[1,3] These behaviors, in addition to the adsorbed surface contaminants, Na_{KLL} (Fig. 5(a)) and diffused Au into LCPs may be responsible for the change of the impedance of Au. The increased impedance for the Pt electrode may be associated with the large number of pores.[31,45,47,49] Also, the interfacial oxidation of Ti (adhesion layer), the delamination of the Pt electrode as well as the diffusion of Pt into LCPs in the Pt electrode system may be attributed to the change of the impedance. In fact, the oxidation of the adhesion layer in all the electrode systems, confirmed by XPS depth profiles, may cause increased impedance of all the electrodes.

Ti showed a similar change in the impedance to that of Pt due to the large number of pores that are infused from the surface through the interface to the LCP. On the other hand,

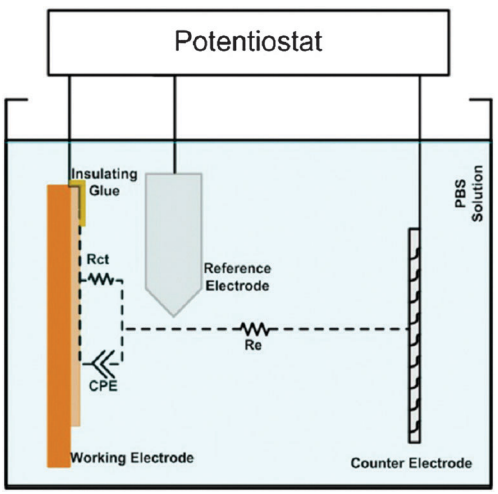

Fig. 8 Schematic diagram of the set-up for electrochemical impedance measurements with an equivalent electrical circuit of the electrode/electrolyte interface.[1] CPE stands for constant phase element and R_{ct} stands for charge transfer resistance.

the lowest contact angle of the Ti electrode was due to its continuous oxides. The Ti electrode showed similar behavior of the impedance to that of Pt due to the continuous oxidation from the electrode into the interfacial region and the presence of pores through the interface. Therefore, the distinct behavior of the impedances for different electrodes at higher frequencies is due to the influence of the oxidation that affected the double layer capacitance associated with the frequency of the electrical signal.

5. Conclusion

The electrochemical impedances of long-term immersed Au, Pt and Ti electrodes in PBS solution decreased at lower frequencies, but increased at higher frequencies compared with those of the short-term immersed electrodes. The increased impedance of the Au electrode could not be explained in terms of its oxide-free surface and pore-free interface. This increase could be due to the oxidation of the adhesion layer in the Au electrode system. For Pt, the increased impedance may be associated with the largest number of pores among the electrodes, the oxidation of the adhesion layer, the delamination of the electrode or the diffusion of the electrode into LCP. The alkali ion (sodium) in the PBS solution might permeate through the pores and attack the oxidized Ti adhesion layer, resulting in the delamination of the Pt electrode. Similar changes in the impedance for the Ti electrode to that of Pt were due to a larger number of pores than that of Au infused from the surface through the interface to LCPs. The oxidation of the adhesion layer identified from the XPS spectra for all the electrode systems considerably influences the increase of the impedances. The adhesion layer was continuously oxidized only for the Ti electrode. Also, while alkali ions (sodium) were present only on the surfaces of Au and Pt electrodes and they penetrated the Ti electrode from the surface all the way to the LCP. The XPS depth profile indicates diffusion of all the electrode materials into the LCP. Further research is needed to investigate the mechanisms for the diffusion. In summary, the oxidation of the adhesion layer, the formation of pores on the surface and interface and the diffusion of the electrode materials into the electrodes and the substrate influence not only the impedance of the implantable electrodes, but also their charge transfer characteristics.

Acknowledgements

This research is supported by Discovery Grants from the Natural Science and Engineering Research Council (NSERC) of Canada, an infrastructure grant from the Canada Foundation for Innovation, an Ontario Research Fund for Research Excellence Funding Grant, a FedDev of Southern Ontario grant, the Canada Research Chair program, and grants from NCE IC-IMPACTS and NSERC Strategic Network Res'Eau. The authors acknowledge Saba Mohtashami and Fangfang Zhang for their help in the fabrication of the electrodes and the measurements of the electrochemical impedance, water contact angle and X-ray photoelectron spectroscopy. The authors also acknowledge Professors Thomas E. Doyle and Joey R. Kish of McMaster University for their contributions to this work.

References

1 M. M. R. Howlader, T. E. Doyle, S. Mohtashami and J. R. Kish, *Sens. Actuators, B*, 2013, **178**, 132–139.
2 K. Wang, C. Liu and D. M. Durand, *IEEE Trans. Biomed. Eng.*, 2009, **56**, 6–14.
3 S. Mohtashami, *Electrochemical Properties of Flexible Electrodes for Implanted Neuromuscular Excitation Applications*, MASc thesis, McMaster University, 2011.
4 S. Mohtashami, M. M. R. Howlader and T. Doyle, *ECS Trans.*, 2011, **35**, 23–33.
5 M. W. Shinwari, M. J. Deen and D. Landheer, *Microelectron. Reliab.*, 2007, **47**, 2025–2057.
6 S.-L. Wu, *et al.*, *Electrochim. Acta*, 2014, **131**, 3–12.
7 L. A. Geddes and R. Roeder, *Ann. Biomed. Eng.*, 2003, **31**, 879–890.
8 M. W. Shinwari and M. J. Deen, *J. Electrochem. Soc.*, 2011, **158**, J189–J194.
9 M. W. Shinwari, M. J. Deen, E. B. Starikov and G. Cuniberti, *Adv. Funct. Mater.*, 2010, **20**, 1865–1883.
10 B. Rubehn and T. Stieglitz, *Biomaterials*, 2010, **31**, 3449–3458.
11 C. Lin, Y. Lee, S. Yeh and W. Fang, *Biosens. Bioelectron.*, 2009, **24**, 2791–2797.
12 N. Chou, S. Yoo and S. Kim, *IEEE Trans. Neural Syst. Rehabil. Eng.*, 2013, **21**, 544–553.
13 Y. Qin, M. M. R. Howlader, M. J. Deen, Y. M. Haddara and P. R. Selvaganapathy, *Sens. Actuators, B*, 2014, **202**, 758–778.
14 K. Jayaraj and B. Farrell, *Advancing Mincroelectronics Magazine*, 1998, **25**, 15–18.
15 T. Suga, A. Takahashi, M. Howlader, K. Saijo and S. Oosawa, *POLYTRONIC 2002 Second International IEEE Conference on Polymers and Adhesives in Microelectronics and Photonics*, Zalaegerszeg, Hungary, 2002, pp. 177–182.
16 M. M. R. Howlader, T. Suga, A. Takahashi, K. Saijo, S. Ozawa and K. Nanbu, *J. Mater. Sci.*, 2005, **40**, 3177–3184.
17 M. M. R. Howlader, M. Iwashita, K. Nanbu, K. Saijo and T. Suga, *IEEE Trans. Adv. Packag.*, 2005, **28**, 495–502.
18 S. Bauer, P. Schmuki, K. Mark and J. Park, *Prog. Mater. Sci.*, 2013, **58**, 261–326.
19 J. D. Weiland, D. J. Anderson and M. S. Humayun, *IEEE Trans. Biomed. Eng.*, 2002, **49**, 1574–1579.
20 E. Jan, J. L. Hendricks, V. Husaini, S. M. Richardson-Burns, A. Sereno, D. C. Martin and N. A. Kotov, *Nano Lett.*, 2009, **9**, 4012–4018.
21 A. M. Dymond, *IEEE Trans. Biomed. Eng.*, 1976, **23**, 274–280.
22 K. Kang, I. S. Choi and Y. Nam, *Biomaterials*, 2011, **32**, 6374–6380.
23 F. Keohan, X. F. Wei, A. Wongsarnpigoon, E. Lazaro, J. E. Darga and W. M. Grill, *J. Biomater. Sci.*, 2007, **18**, 1057–1073.

24 S. A. Fadl-allaha and Q. Mohsen, *Appl. Surf. Sci.*, 2010, **256**, 5849–5855.
25 S. Musa, D. R. Rand, D. J. Cott, J. Loo, C. Bartic, W. Eberle, B. Nuttin and G. Borghs, *ACS Nano*, 2012, **6**, 4615–4628.
26 S. L. Morton, M. L. Daroux and J. T. Mortimer, *Electrochem. Soc. Jpn.*, 1994, **141**, 122–130.
27 J. Riistama and J. Lekkala, *Proceedings of IEEE Engineering Medical Biology Society*, 2006, pp. 6021–6024.
28 H. Gensler, R. Sheybani, P.-Y. Li, R. Lo, S. Zhu, K.-T. Yong, I. Roy, P. N. Prasad, R. Masood, U. K. Sinha and E. Meng, *IEEE 23rd International Conf. on Micro-Electro- Mechanical Systems (MEMS)*, 2010, pp. 23–26.
29 A. Bozkurt, *IEEE Topical Conf. on Biomedical Wireless Technologies, Networks, and Sensing Systems (BioWireleSS)*, 2012, pp. 45–48.
30 A. S. Widge, *Self-Assembled Monolayers of Polythiophene "Molecular Wires": A New Electrode Technology for Neuro-Robotic Interfaces*, Doctoral thesis, CMU-RI-TR-07-03, 2007.
31 A. Alam, M. M. R. Howlader and M. Deen, *J. Micromech. Microeng.*, 2014, **24**, 035010.
32 S. B. Hall, E. A. Khudaish and A. L. Hart, *Electrochim. Acta*, 1998, **43**, 2015–2024.
33 S. Andreescu, D. Andreescu and O. A. Sadik, *Electrochem. Commun.*, 2003, **5**, 681–688.
34 S. Tamilselvi, R. Murugaraj and N. Rajendran, *Mater. Corros.*, 2007, **58**, 113–120.
35 A. B. Majji, M. S. Humayun, J. D. Weiland, S. Suzuki, S. A. D'Anna and E. de Juan, *Invest. Ophthalmol. Visual Sci.*, 1999, **40**, 2073–2081.
36 A. Santos, M. J. Deen and L. F. Marsal, *Nanotechnology*, 2015, **26**, 042001.
37 M. J. Deen and F. Pascal, *J. Mater. Sci.: Mater. Electron.*, 2006, **17**, 549–575.
38 M. M. R. Howlader, J. G. Wang and M. J. Kim, *Mater. Lett.*, 2010, **64**, 445–448.
39 A. Dimitrov, P. Kralchevsky, A. Nikolov, H. Noshi and M. Matsumoto, *J. Colloid Interface Sci.*, 1991, **145**, 279–282.
40 Sonoscan, Sonoscan GEN5 C-SAM Operation & Maintenance Manual, 2007.
41 CasaXPS Manual 2.3.15 Rev 1.2. Link: http://www.casaxps.com/ebooks/XPS%20AES%20Book%20new%20margins%20rev%201.2%20for%20web.pdf.
42 J.-B. Jorcin, M. E. Orazem, N. Pebere and B. Tribollet, *Electrochim. Acta*, 2006, **51**, 1473–1479.
43 M. M. R Howlader, G. Kagami, S. H. Lee, J. G. Wang, M. Kim and A. Yamauchi, *J. Microelectromech. Syst.*, 2010, **19**, 840–848.
44 M. G. Kibria, F. Zhang, T. H. Lee, M. J. Kim and M. M. R. Howlader, *Nanotechnology*, 2010, **21**, 134011.
45 H. Nakae, R. Inui, Y. Hirata and H. Saito, *Acta Mater.*, 1998, **46**, 2313–2318.
46 K. W. Bewig and W. A. Zisman, *J. Phys. Chem.*, 1965, **69**, 4238–4242.
47 N. Eliaz, S. Shmueli, I. Shur, D. Benayahu, D. Aronov and G. Rosenman, *Acta Biomater.*, 2009, **5**, 3178–3191.
48 A. Norlin, J. Pan and C. Leygrafa, *J. Electrochem. Soc.*, 2005, **152**, J7–J15.
49 C. Liu, Q. Bi, A. Leyland and A. Matthews, *Corros. Sci.*, 2003, **45**, 1257–1273.
50 A. U. Alam, M. M. R. Howlader and M. J. Deen, *ECS J. Solid State Sci. Technol.*, 2013, **2**, 515–523.
51 M. M. R. Howlader, F. Zhang and M. J. Deen, *Nanotechnology*, 2013, **24**, 315301.
52 J. Hoogvliet and W. Bennekom, *Electrochim. Acta*, 2001, **47**, 599–611.
53 U. Oesch and J. Janata, *Electrochim. Acta*, 1983, **28**, 1247–1253.
54 A. Tlili, A. Abdelghani, S. Hleli and M. A. Maaref, *Sensors*, 2004, **4**, 105–114.
55 E. M. Hudak, J. T. Mortimer and H. B. Martin, *Journal of Neural Engineering*, 2010, **7**, 026005.
56 S. Musa, D. R. Rand, C. Bartic, W. Eberle, B. Nuttin and G. Borghs, *Anal. Chem.*, 2011, **83**, 4012–4022.
57 J. Pan, D. Thierry and C. Leygraft, *Electrochim. Acta*, 1996, **41**, 1143–1153.
58 J. Pan, D. Thierry and C. Leygraft, *J. Biomed. Mater. Res.*, 1994, **28**, 113–122.